# Antiresonance in the spin current through a quantum dot induced by electron-phonon interaction

Li-Ling Zhou,[1,2,*] Zhao-Yang Zeng,[3] Xue-Yun Zhou,[1,2] and Yi-Gao Wang[1,2]
[1]*Department of Physics, Jiujiang University, Jiujiang 332005, China*
[2]*Jiangxi Province Key Lab of Microstructure Functional Materials, Jiujiang 332005, China*
[3]*Department of Physics, Jiangxi Normal University, Nanchang 330022, China*

(Received 10 February 2020; revised 6 July 2020; accepted 7 July 2020; published 22 July 2020)

We investigate the nonequilibrium spin transport through an electron-phonon coupled quantum dot, on which an external magnetic field $B_0$ and a rotating magnetic field $[B_1\cos(\omega_1 t), B_1\sin(\omega_1 t)]$ are applied. It is found that the spin current is significantly affected by the destructive interference between electron tunneling waves through different spin channels. As a result, dips appear in the spin current as a function of $\omega_1$ every time the Rabi frequency is tuned to be integral numbers of the phonon frequency. It is also found that the main spin current peak does not always exist at the resonant rotating frequency $\omega_1 = g\mu_B B_0$.

DOI: 10.1103/PhysRevB.102.045422

## I. INTRODUCTION

The electron-phonon interaction (EPI) determines a variety of physical properties of nanodevices. It induces long-lasting nonequilibrium in the electron system of a laser-excited solid [1] and leads to degeneracy lifting of Majorana bound states [2]. The transport properties of nanosystems have been found to be profoundly impacted by the EPI [3–14]. Vibronic structures appear in transport characteristics because of the phonon satellites arising in spectral functions of nanosystem electrons [7,9,14]. Replicas of the Kondo effect appear in the conductance through a molecule or a quantum dot in which the occupation of the relevant electronic level is coupled to a phonon mode [4]. In a double-quantum-dot system the interplay between strong electron-phonon coupling and interdot tunneling can lead to a negative differential conductance [5].

Characteristics arising from EPI are naturally expected in spin current or spin-dependent transports through a nanodevice [15]. The mesoscopic quantum dots are one of the most important spin-based electronic devices and are known as ideal systems for a detailed investigation of electronic transport phenomena. Because of the small size of the dots, electron transport is influenced significantly by nuclear vibrational degrees of freedom, i.e., phonons, which has been observed in a variety of experiments [16–24].

## II. MODEL AND FORMULATION

In this paper, we investigate the spin current through a single-level quantum dot (QD), in which electrons are coupled to a single-mode phonon bath. The single level is split by an external magnetic field $B_0$, $\varepsilon_\downarrow - \varepsilon_\uparrow = \omega_r = g\mu_B B_0$, with $g$ being the effective electron gyromagnetic factor and $\mu_B$ being the Bohr magneton. The spins are coupled by a rotating magnetic field $[B_1 cos(\omega_1 t), B_1 sin(\omega_1 t)]$ applied perpendicular to $B_0$. Spin current is generated as the QD couples to an electron reservoir. The model Hamiltonian can be written as $H = H_{\rm dot} + H_{\rm Lead} + H_T$ (hereafter $\hbar = 1$). Here,

$$H_{\rm dot} = \sum_\sigma [\varepsilon_\sigma + \lambda(b^\dagger + b) + U d^\dagger_{\bar\sigma} d_{\bar\sigma}/2] d^\dagger_\sigma d_\sigma - g\mu_B B_1 (d^\dagger_\uparrow d_\downarrow e^{i\omega_1 t} + d^\dagger_\downarrow d_\uparrow e^{-i\omega_1 t}) + \omega_0 b^\dagger b \quad (1)$$

describes the QD state. $H_{\rm Lead} = \sum_{k\sigma} \varepsilon_k a^\dagger_{k\sigma} a_{k\sigma}$ represents a normal-metal lead. $H_T = \sum_{k\sigma}(V a^\dagger_{k\sigma} d_\sigma + {\rm H.c.})$ depicts hybridization between the QD and the lead. The fermion operators $d^\dagger_\sigma$ ($d_\sigma$) and $a^\dagger_{k\sigma}$ ($a_{k\sigma}$) create (annihilate) an electron of spin $\sigma = \uparrow, \downarrow$ in the QD and the lead, respectively, and the bosonic operator $b^\dagger$ ($b$) creates (destroys) a phonon mode of frequency $\omega_0$ in the QD. Here, $\lambda$ and $U$ are the respective strengths of EPI and intradot $e$-$e$ Coulomb repulsion.

By introducing a unitary transformation $U = \exp\{\frac{-i\omega_1 t}{2}[(d^\dagger_\downarrow d_\downarrow - d^\dagger_\uparrow d_\uparrow) + \sum_k (a^\dagger_{k\downarrow} a_{k\downarrow} - a^\dagger_{k\uparrow} a_{k\uparrow})]\}$, we can eliminate the time dependence of Hamiltonian $H$ while transforming the system into the rotating reference,

$$\begin{aligned} H^{rf} &= U^{-1} H U + i(\partial_t U^{-1}) U \\ &= \sum_\sigma [\varepsilon^{rf}_\sigma + \lambda(b^\dagger + b) + U d^\dagger_{\bar\sigma} d_{\bar\sigma}/2)] d^\dagger_\sigma d_\sigma \\ &\quad - g\mu_B B_1 (d^\dagger_\uparrow d_\downarrow + d^\dagger_\downarrow d_\uparrow) + \omega_0 b^\dagger b \\ &\quad + \sum_{k\sigma} \varepsilon^{rf}_{k\sigma} a^\dagger_{k\sigma} a_{k\sigma} + \sum_{k\sigma} (V a^\dagger_{k\sigma} d_\sigma + {\rm H.c.}), \end{aligned} \quad (2)$$

where $\varepsilon^{rf}_{\uparrow(\downarrow)} = \varepsilon_{\uparrow(\downarrow)} \pm \frac{\omega_1}{2}$ and $\varepsilon^{rf}_{k\uparrow(\downarrow)} = \varepsilon_k \pm \frac{\omega_1}{2}$ are the shifted QD and lead electronic energies for up and down spins. The spin splitting of lead electron energy is induced by hybridization between the QD level and conduction channel, which propagates energy from the QD to the lead and then generates spin chemical potentials $\mu_{\uparrow,\downarrow} = \mp\omega_1/2$ in the lead. In spite of a spin imbalance, the charge chemical potential is still $\mu = (\mu_\uparrow + \mu_\downarrow)/2 = 0$. Due to the one-photon difference between $\mu_\downarrow$ and $\mu_\uparrow$, an electron in the spin-down channel of the lead can tunnel into the level $\varepsilon^{rf}_\downarrow$ in the QD and then tunnel out

*147667896@qq.com

 

into the spin-up channel after experiencing a spin-flip process given by the rotating magnetic field. This tunneling process repeats, and then a steady spin current builds up.

In the absence of hybridization and Coulomb repulsion, the QD is reduced to a simple driven two-level system. It is characterized by a coherent weight transfer, Rabi oscillation, between the two spin states, which is complete as $\omega_1$ is tuned to $\omega_1 = \omega_r$. The spin oscillation period is $T = 2\pi/\Omega$, with $\Omega = \sqrt{\Delta^2 + (2g\mu_B B_1)^2}$ being the Rabi frequency and $\Delta = \omega_r - \omega_1$ representing the detuning from the resonance.

We simplify the Hamiltonian (2) by introducing a new set of Fermi operators, $\{c_\uparrow, c_\downarrow\}$, which is related to $\{d_\uparrow, d_\downarrow\}$ by

$$\begin{pmatrix} d_\uparrow \\ d_\downarrow \end{pmatrix} = S \begin{pmatrix} c_\uparrow \\ c_\downarrow \end{pmatrix}, \quad S = \begin{pmatrix} \cos\theta & -\sin\theta \\ \sin\theta & \cos\theta \end{pmatrix}, \tag{3}$$

with $\theta = \frac{1}{2}\arctan(2g\mu_B B_1/\Delta)$. In terms of the new operators, the QD electronic states are diagonal, and the Hamiltonian (2) turns into

$$\begin{aligned} H_c^{rf} &= \sum_\sigma \varepsilon_{c\sigma}^{rf} c_\sigma^\dagger c_\sigma + \lambda(b^\dagger + b)\sum_\sigma c_\sigma^\dagger c_\sigma + U c_\uparrow^\dagger c_\uparrow c_\downarrow^\dagger c_\downarrow \\ &\quad + \omega_0 b^\dagger b + \sum_{k\sigma} \varepsilon_{k\sigma}^{rf} a_{k\sigma}^\dagger a_{k\sigma} \\ &\quad + \sum_{k\sigma\sigma'} (V a_{k\sigma}^\dagger S_{\sigma\sigma'} c_{\sigma'} + \text{H.c.}), \end{aligned} \tag{4}$$

where $\varepsilon_{c\uparrow(\downarrow)}^{rf} = (\varepsilon_\uparrow + \varepsilon_\downarrow \mp \Omega)/2 = \varepsilon_0 \mp \Omega/2$ for the up and down spins. In the $H_c^{rf}$ frame, spin-flip events can occur when an electron tunnels into or out of the QD, and electron-phonon interaction may take place in the QD. Using the nonequilibrium Green's functions of the QD [25], we can obtain the spin-$\sigma$ current, say, the spin-$\uparrow$ current,

$$I_\uparrow = i\text{Tr}\int \frac{d\omega}{2\pi} \mathbf{\Gamma}_\uparrow \{[1 - f_\uparrow(\omega)]\mathbf{G}^<(\omega) + f_\uparrow(\omega)\mathbf{G}^>(\omega)\}, \tag{5}$$

where

$$\mathbf{\Gamma}_\uparrow = \Gamma \begin{pmatrix} \cos^2\theta & -\sin\theta\cos\theta \\ -\sin\theta\cos\theta & \sin^2\theta \end{pmatrix}, \tag{6}$$

with $\Gamma = 2\pi|V|^2 \sum_k \delta(\omega - \varepsilon_k)$ being the linewidth and assumed to be independent of energy $\omega$. $f_\sigma(\omega) = \{\exp[(\omega - \mu_\sigma)/\kappa_B T] + 1\}^{-1}$ is the Fermi distribution function for the spin $\sigma$ channel. $\mathbf{G}^{<,>}(\omega)$ are the Fourier transformations of the lesser and greater Green's functions of the QD,

$$\mathbf{G}^{<,>}(t) = \begin{pmatrix} G_{\uparrow\uparrow}^{<,>}(t) & G_{\uparrow\downarrow}^{<,>}(t) \\ G_{\downarrow\uparrow}^{<,>}(t) & G_{\downarrow\downarrow}^{<,>}(t) \end{pmatrix},$$

with the matrix elements being defined as $G_{\sigma\sigma'}^<(t) = i\langle c_{\sigma'}^\dagger(0) c_\sigma(t)\rangle$ and $G_{\sigma\sigma'}^>(t) = -i\langle c_\sigma(t) c_{\sigma'}^\dagger(0)\rangle$.

The EPI in the dot can be eliminated by introducing a canonical transformation: $\widetilde{H}_{\text{cdot}}^{rf} = e^S H_{\text{cdot}}^{rf} e^{-S}$, with $S = \lambda/\omega_0(b^\dagger - b)\sum_\sigma c_\sigma^\dagger c_\sigma$ and the dot Hamiltonian $H_{\text{cdot}}^{rf} = \sum_\sigma \varepsilon_{c\sigma}^{rf} c_\sigma^\dagger\ c_\sigma + \lambda(b^\dagger + b)\sum_\sigma c_\sigma^\dagger c_\sigma\ + U c_\uparrow^\dagger\ c_\uparrow\ c_\downarrow^\dagger\ c_\downarrow + \omega_0 b^\dagger b$. Under this transformation, the electron operator $c_\sigma$ and the phonon operator $b$ are transformed to

$$\begin{aligned} \tilde{c}_\sigma &= e^S c_\sigma e^{-S} = c_\sigma X, \\ \tilde{b} &= e^S b e^{-S} = b - \lambda/\omega_0 \sum_\sigma c_\sigma^\dagger c_\sigma, \end{aligned} \tag{7}$$

where $X = \exp[-\lambda/\omega_0(b^\dagger - b)]$. Replacing the operators $c_\sigma$ and $b$ in $H_{\text{cdot}}^{rf}$ with $\tilde{c}_\sigma$ and $\tilde{b}$, respectively, we get straightforwardly the transformed, electron-phonon interaction decoupled dot Hamiltonian,

$$\widetilde{H}_{\text{cdot}}^{rf} = \sum_\sigma \tilde{\varepsilon}_{c\sigma}^{rf} c_\sigma^\dagger c_\sigma + \widetilde{U} c_\uparrow^\dagger c_\uparrow c_\downarrow^\dagger c_\downarrow + \omega_0 b^\dagger b, \tag{8}$$

with $\tilde{\varepsilon}_{c\sigma}^{rf} = \varepsilon_{c\sigma}^{rf} - \lambda^2/\omega_0$ and $\widetilde{U} = U - 2\lambda^2/\omega_0$, with $\lambda^2/\omega_0$ being the electron self-energy. For simplicity we consider the case of vanishing effective charge energy, $\widetilde{U} = 0$. By applying this canonical transformation, the retarded Green's function $\mathbf{g}^r(\omega)$ for the isolated dot, described by $H_{\text{cdot}}^{rf}$, can be calculated exactly [26]. Take, for example, the matrix element $\mathbf{g}_{11}^r(\omega)$, which is the Fourier transformation of $\mathbf{g}_{11}^r(t)$, i.e., $g_{\uparrow\uparrow}^r(t)$,

$$\begin{aligned} g_{\uparrow\uparrow}^r(t) &= -i\theta(t)\langle\{c_\uparrow(t), c_\uparrow^\dagger(0)\}\rangle \\ &= -i\theta(t)[\langle c_\uparrow(t) c_\uparrow^\dagger(0)\rangle + \langle c_\uparrow^\dagger(0) c_\uparrow(t)\rangle]. \end{aligned} \tag{9}$$

By inserting the factor $1 = e^{-S}e^S$ we can transform $g_{\uparrow\uparrow}^r(t)$ from the $H_{\text{cdot}}^{rf}$ representation to the $\widetilde{H}_{\text{cdot}}^{rf}$ frame. Consider, for example, the first term in the square brackets in Eq. (9),

$$\begin{aligned} \langle c_\uparrow(t) c_\uparrow^\dagger(0)\rangle_{H_{\text{cdot}}^{rf}} &= e^{\beta\Omega}\text{Tr}[e^{-\beta H_{\text{cdot}}^{rf}} e^{iH_{\text{cdot}}^{rf}t} c_\uparrow(0) e^{-iH_{\text{cdot}}^{rf}t} c_\uparrow^\dagger(0)] \\ &= e^{\beta\Omega}\text{Tr}[e^{-\beta\widetilde{H}_{\text{cdot}}^{rf}} e^{i\widetilde{H}_{\text{cdot}}^{rf}t} \tilde{c}_\uparrow(0) e^{-i\widetilde{H}_{\text{cdot}}^{rf}t} \tilde{c}_\uparrow^\dagger(0)] \\ &= \langle \tilde{c}_\uparrow(t) \tilde{c}_\uparrow^\dagger(0)\rangle_{\widetilde{H}_{\text{cdot}}^{rf}}. \end{aligned} \tag{10}$$

Here, in the third line the factor $e^{-S}e^S$ is inserted, and the cyclic property of the trace is used. Since in $\widetilde{H}_{\text{cdot}}^{rf}$ there is no interaction between the electron part $\widetilde{H}_{el} = \sum_\sigma \tilde{\varepsilon}_{c\sigma}^{rf} c_\sigma^\dagger c_\sigma$ and the phonon part $\widetilde{H}_{\text{ph}} = \omega_0 b^\dagger b$, after putting $\tilde{c}_\sigma = c_\sigma X$ and $\tilde{c}_\sigma^\dagger = c_\sigma^\dagger X^\dagger$ explicitly, Eq. (10) can be written as

$$\begin{aligned} \langle c_\uparrow(t) X(t) c_\uparrow^\dagger(0) X^\dagger(0)\rangle_{\widetilde{H}_{\text{cdot}}^{rf}} &= \langle c_\uparrow(t) c_\uparrow^\dagger(0)\rangle_{\widetilde{H}_{el}} \langle X(t) X^\dagger(0)\rangle_{\widetilde{H}_{\text{ph}}} \\ &= (1 - n_\uparrow) e^{-i\tilde{\varepsilon}_{c\uparrow}^{rf} t} e^{-\Phi(t)}. \end{aligned} \tag{11}$$

$n_\uparrow$ is the number of spin-up electrons in the QD. $\Phi(t) = g[N_{\text{ph}}(1 - e^{i\omega_0 t}) + (N_{\text{ph}} + 1)(1 - e^{-i\omega_0 t})]$, with $g = (\lambda/\omega_0)^2$ and the number of phonons $N_{\text{ph}} = 1/\{\exp[\omega_0/(\kappa_B T_{\text{ph}})] - 1\}$, where $T_{\text{ph}}$ is the phonon temperature. Evaluating the second term in the same way, we find

$$\langle c_\uparrow^\dagger(0) c_\uparrow(t)\rangle_{H_{\text{cdot}}^{rf}} = n_\uparrow e^{-i\tilde{\varepsilon}_{c\uparrow}^{rf} t} e^{-\Phi(-t)}. \tag{12}$$

Substituting the results of Eqs. (11) and (12) into Eq. (9) and then transforming this equation to the energy space, we have

$$\begin{aligned} g_{\uparrow\uparrow}^r(\omega) = \sum_{n=-\infty}^{\infty} L_n \Bigg( &\frac{1 - n_\uparrow}{\omega - \tilde{\varepsilon}_{c\uparrow}^{rf} - n\omega_0 + i0^+} \\ &+ \frac{n_\uparrow}{\omega - \tilde{\varepsilon}_{c\uparrow}^{rf} + n\omega_0 + i0^+} \Bigg). \end{aligned} \tag{13}$$

Here, the identity $e^{-\Phi(t)} = \sum_{n=-\infty}^{\infty} L_n e^{-in\omega_0 t}$ is used. The Franck-Condon factor $L_n \equiv e^{-g(2N_{\rm ph}+1)} e^{n\omega_0/(2\kappa_B T_{\rm ph})} I_n[2g\sqrt{N_{\rm ph}(N_{\rm ph}+1)}]$, with $I_n(z)$ being the $n$th Bessel function of the complex argument $z$. Here, $0^+$ is a positive infinitesimal.

In the same way, we can get

$$g^r_{\downarrow\downarrow}(\omega) = \sum_{n=-\infty}^{\infty} L_n \Bigg( \frac{1-n_\downarrow}{\omega - \tilde{\varepsilon}^{rf}_{c\downarrow} - n\omega_0 + i0^+} + \frac{n_\downarrow}{\omega - \tilde{\varepsilon}^{rf}_{c\downarrow} + n\omega_0 + i0^+} \Bigg). \tag{14}$$

The nondiagonal elements of $\mathbf{g}^r(\omega)$ are easily found to be zero, $g^r_{\uparrow\downarrow}(\omega) = g^r_{\downarrow\uparrow}(\omega) = 0$.

The retarded Green's function $\mathbf{G}^r(\omega)$ of the QD in the presence of QD-lead coupling is given by $G^r_{\uparrow\downarrow}(\omega) = G^r_{\downarrow\uparrow}(\omega) = 0$ and $G^r_{\uparrow\uparrow(\downarrow\downarrow)}(\omega) = [\mathbf{g}^{r-1}(\omega) - \mathbf{\Sigma}^r(\omega)]^{-1}_{11(22)}$, where the retarded self-energy is $\mathbf{\Sigma}^r(\omega) = -i\Gamma\mathbf{I}/2$, which is contributed by electron tunneling between the QD and lead. The lesser and greater Green's functions can be obtained via the Keldysh equation, $\mathbf{G}^{<,>}(\omega) = \mathbf{G}^r(\omega)\mathbf{\Sigma}^{<,>}(\omega)\mathbf{G}^a(\omega)$, with the advanced Green's function $\mathbf{G}^a(\omega) = \mathbf{G}^{r*}(\omega)$ and the lesser self-energy matrix

$$\mathbf{\Sigma}^<(\omega) = i\Gamma \begin{pmatrix} \cos^2\theta f_\uparrow(\omega) + \sin^2\theta f_\downarrow(\omega) & \sin\theta\cos\theta[f_\downarrow(\omega) - f_\uparrow(\omega)] \\ \sin\theta\cos\theta[f_\downarrow(\omega) - f_\uparrow(\omega)] & \sin^2\theta f_\uparrow(\omega) + \cos^2\theta f_\downarrow(\omega) \end{pmatrix}. \tag{15}$$

The greater self-energy matrix $\mathbf{\Sigma}^>(\omega)$ is given directly when the function $f_\sigma(\omega)$ in Eq. (15) is replaced by $f_\sigma(\omega) - 1$. From the equation $n_{\uparrow,\downarrow} = \int \frac{d\omega}{2\pi} \mathrm{Im}\mathbf{G}^<_{11,22}(\omega)$ the electron numbers are self-consistently solved.

Substitution of the expression of $\mathbf{G}^{<,>}(\omega)$ into Eq. (5) gives the expression of spin-up current,

$$I_\uparrow = \Gamma^2 \mathrm{Tr} \int \frac{d\omega}{2\pi} \boldsymbol{\tau}_y \mathbf{u} \boldsymbol{\tau}_y \mathbf{G}^r(\omega) \mathbf{u} \mathbf{G}^a(\omega) \{f_\uparrow(\omega) - f_\downarrow(\omega)\}, \tag{16}$$

where $\mathbf{u}_{11(22)} = \sin^2\theta(\cos^2\theta)$, $\mathbf{u}_{12(21)} = \sin\theta\cos\theta$, and $\boldsymbol{\tau}_y$ is the $y$ component of the Pauli matrix vector. The total spin current through the QD is defined as $I_s = I_\downarrow - I_\uparrow = -2I_\uparrow$, and the spectral function of the QD electron of spin $\sigma$ is $A_\sigma(\omega) = -\mathrm{Im}[G^r_{\sigma\sigma}(\omega) - G^a_{\sigma\sigma}(\omega)]$.

## III. RESULTS AND DISCUSSION

In previous studies, current exhibits satellite peaks due to EPI [9,11,13,14]. However, in Fig. 1, which shows the spin current as a function of the rotating frequency $\omega_1$, dips, instead of peaks, appear in each curve when the Rabi frequency $\Omega$ is tuned to be an integral number of one phonon quantum $\omega_0$. At each dip the corresponding $\Omega$ value is marked. We attribute this phenomenon to the destructive interference between electron tunneling waves through the spin-up channel of the QD and that through the spin-down channel. In the $\widetilde{H}^{rf}_{\rm cdot}$ picture, an electron of spin down of the lead can tunnel into the spin-down channel in the QD and then tunnels out with spin flip. It can also transfer the dot via the spin-up channel with spin flip occurring as it enters. Equation (4) shows the probability amplitudes for an electron to get spin flipped or not when it tunnels into (or out of) the dot are, respectively, $V\sin\theta$ and $V\cos\theta$.

Figure 2 gives the spectral functions $A(\omega)$ of the QD electron at three specific rotating frequencies, $\omega_1/\omega_0 =$

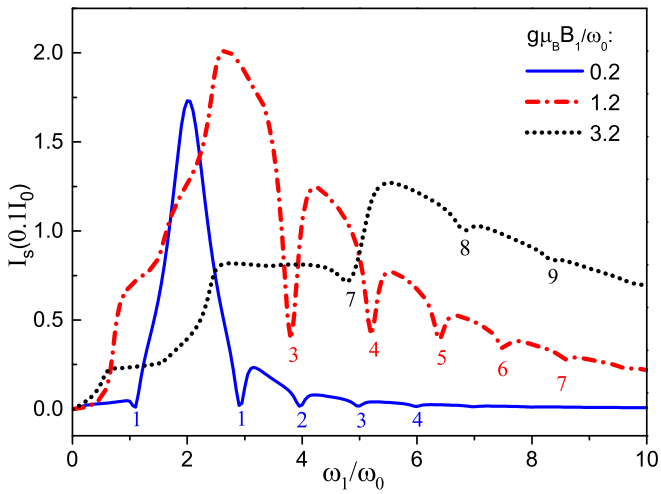


FIG. 1. Spin current at different values of $B_1$ with, in units of $\omega_0$, $\kappa_B T = 0$, $\kappa_B T_{\rm ph} = 5$, $\Gamma = 0.1$, $\lambda = 0.7$, $\omega_r = 2$, $\varepsilon_0 = \lambda^2/\omega_0$, and $I_0 = e\Gamma/\pi\hbar$.

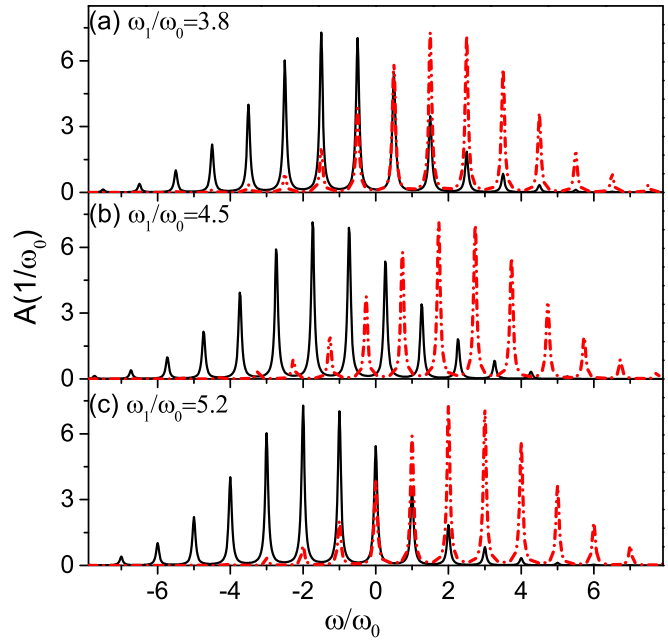


FIG. 2. The dimensionless spectral functions of a QD electron of spin up (solid line) and spin down (dash-dotted line) corresponding to two adjacent dips ($\omega_1/\omega_0 = 3.8, 5.2$) and a peak between in the curve of $g\mu_B B_1/\omega_0 = 1.2$ in Fig. 1.

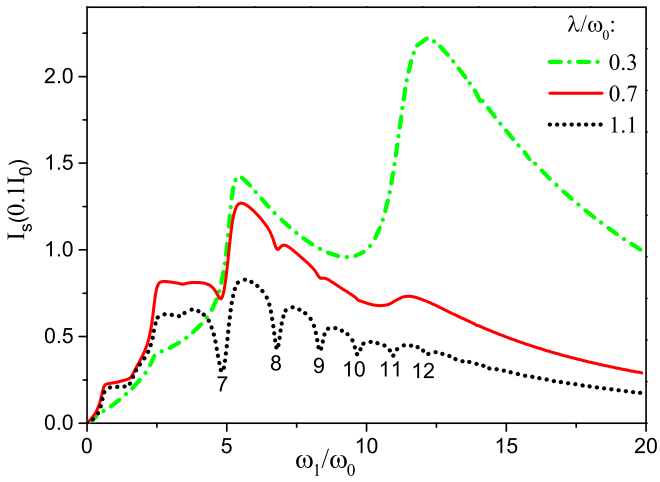


FIG. 3. Spin current dependence of electron-phonon interaction strength $\lambda$ at $g\mu_B B_1 = 3.2\omega_0$. Other parameters are as in Fig. 1

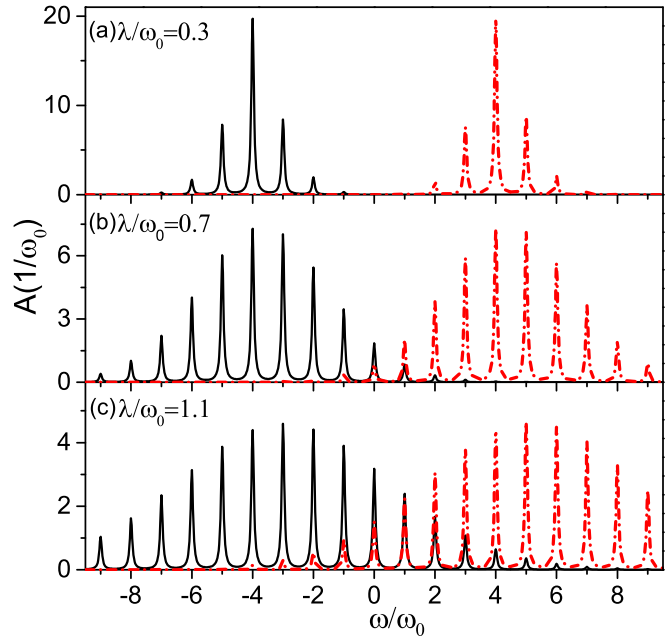


FIG. 4. The dimensionless spectral functions of the QD electron for different EPI strengths $\lambda$ with $\Omega = 8\omega_0$ and $g\mu_B B_1 = 3.2\omega_0$; the solid line is for spin up, and the dash-dotted line is for spin down. Other parameters are as in Fig. 1.

3.8, 4.5, 5.2. At $g\mu_B B_1/\omega_0 = 1.2$ and $\omega_r/\omega_0 = 2$ we have $\Omega/\omega_0 = 3$ for $\omega_1/\omega_0 = 3.8$, $\Omega/\omega_0 = 3.5$ for $\omega_1/\omega_0 = 4.5$, and $\Omega/\omega_0 = 4$ for $\omega_1/\omega_0 = 5.2$. In an $A(\omega) \sim \omega$ curve of spin up (down), the solid black line (dash-dotted red line), a big peak arises at $\omega = \tilde{\varepsilon}^{rf}_{c\uparrow} = -0.5\Omega$ ($\omega = \tilde{\varepsilon}^{rf}_{c\downarrow} = 0.5\Omega$), and due to the EPI, satellite peaks appear at $-0.5\Omega \pm n\omega_0$ ($0.5\Omega \pm n\omega_0$), with $n$ being a positive integer. For later convenience, we label the resonant peak at $\omega = -0.5\Omega$ ($\omega = 0.5\Omega$) the $0_\uparrow$-phonon ($0_\downarrow$-phonon) band and the peaks at $-0.5\Omega \pm n\omega_0$ ($0.5\Omega \pm n\omega_0$) the $\pm n_\uparrow$th ($\pm n_\downarrow$th) phonon sidebands. Figure 2(a) shows that the $3_\uparrow$th band locates at the very place where the $0_\downarrow$ band lies. This is because the gap between energy level $\tilde{\varepsilon}^{rf}_{c\downarrow}$ and level $\tilde{\varepsilon}^{rf}_{c\uparrow}$ is the very value of $3\omega_0$, i.e., $\Omega = 3\omega_0$. Then, the overlap between the spectral function of spin up and that of spin down reaches a maximal value, leading to a maximal intensity of destructive interference between electron waves of different spins. Therefore, at $\omega_1 = 3.8$ a deep dip appears in the $I_s$-$\omega_1$ curve of $g\mu_B B_1/\omega_0 = 1.2$ (see Fig. 1). With $\omega_1$ increasing, these two levels move away from each other. The overlap reduces first and then expands after it reaches a minimal value at about $\Omega = 3.5$, as shown in Fig. 2(b). A second maximal value is generated as $\omega_1$ increases to $\omega_1 = 5.2$ [$\Omega = 4$; see Fig. 2(c)] when the $4_\uparrow$th band and the $0_\downarrow$ one are in the same position. So a second dip emerges at $\omega_1 = 5.2$ in the dash-dotted line in Fig. 1. This dip is not as deep as that at $\omega_1 = 3.8$ because of [compare with Fig. 2(a)] less overlap between spectral functions of different spins in Fig. 2(c). The examples above tell why a dip appears in the $I_s$-$\omega_1$ curves every time $\Omega$ equals $n\omega_0$ and is less deep for larger $n$.

On spin current the effect of intradot electron-phonon interaction strength is shown in Fig. 3. As in Fig. 1, the Arabic numerals below the dot line indicate the level gap $\Omega$ corresponding to each dip. $I_s$ as a function of $\omega_1$ exhibits no dip at all when the EPI is weak, e.g., $\lambda = 0.3\omega_0$. However, dips become visible as the EPI is enhanced to some point, say, $\lambda = 0.7\omega_0$, and these dips are deepened as the EPI strengthens further, as seen in the curve of $\lambda/\omega_0 = 1.1$. The reason is the spectral weight is distributed among an increasing number of phonon bands for increasing $\lambda$, enlarging the overlap between spectral functions of different spins at $\Omega = n\omega_0$, as can be seen in Fig. 4.

The spin current depends mainly on three factors: (1) the total spectral weight contributing to the electron

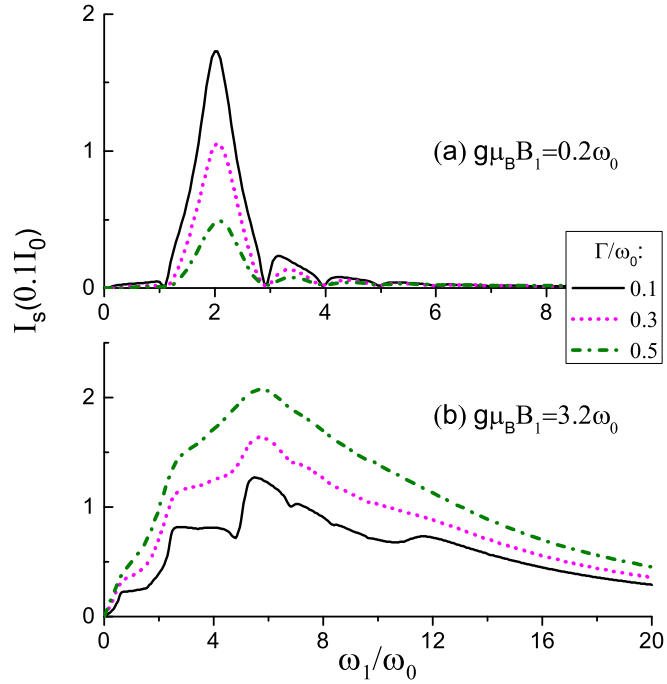


FIG. 5. Spin current dependence of electronic coupling strength between the QD and the lead for (a) $g\mu_B B_1 = 0.2\omega_0$ and (b) $3.2\omega_0$. Other parameters are as in Fig. 1.

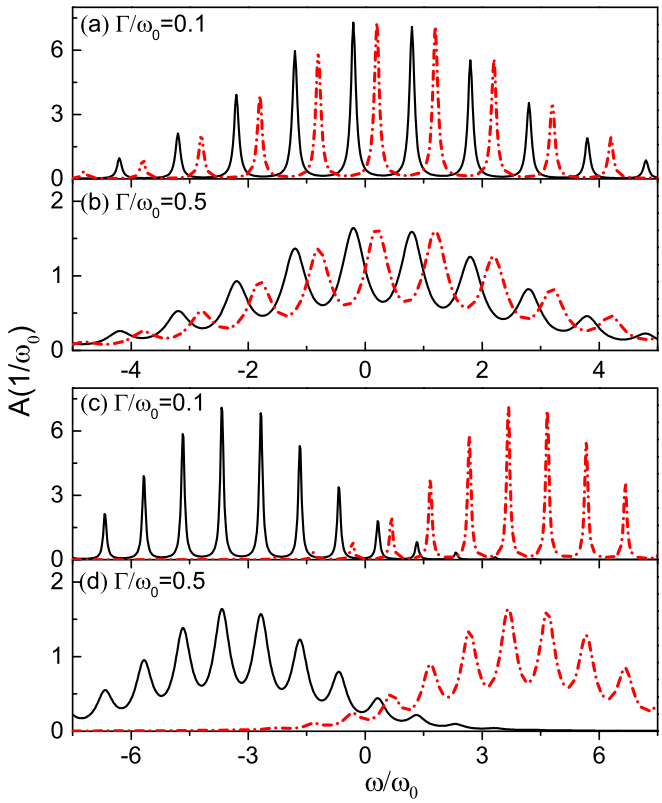


FIG. 6. The dimensionless spectral functions of the QD electron for different $\Gamma$ with $\omega_1 = 2\omega_0$, $g\mu_B B_1 = 0.2\omega_0$ in (a) and (b) and $\omega_1 = 5.6\omega_0$, $g\mu_B B_1 = 3.2\omega_0$ in (c) and (d). The solid line is for spin up, and the dash-dotted line is for spin down. Other parameters are as in Fig. 1.

tunneling process, (2) the intensity of destructive interference between tunneling electron waves passing through different conduction spin channels, and (3) the probability amplitude for an electron to get spin flipped as it traverses the QD, which is $P = V^2 \sin\theta\cos\theta = V^2 g\mu_B B_1/\Omega$. With $\lambda = 0.3\omega_0$ and $g\mu_B B_1 = 3.2\omega_0$, the spectral bands of different spins are completely separated [see Fig. 4(a)]. So no destructive interference occurs, and then no dip appears in the $I_s$-$\omega_1$ curve, as shown in Fig. 3 (dash-dotted line). With rising $\omega_1$ the probability amplitude $P$ goes up first and then down after reaching the maximum value at $\omega_1 = \omega_r$, while the spectral weight contributing to the tunneling process expands monotonically. There is no doubt that $I_s$ increases as $\omega_1$ rises from 0 to $2\omega_0$. However, with $\lambda = 0.3\omega_0$ it keeps increasing until $\omega_1$ rises to about $5.4\omega_0$. This is because the expanding spectral weight dominates the current in this rotating frequency range. During this increase a steep rise occurs at around $\omega_1 = 5\omega_0$, which results from the $-1_\downarrow$th and $1_\uparrow$th bands entering the bias window. As $\omega_1$ rises further, the diminishing $P$ dominates $I_s$ until the $0_\downarrow$ and $0_\uparrow$ bands enter the bias window, which brings about a big spin current peak at $\omega_1$ slightly larger than $11\omega_0$. After this, $P$ dominates again, and $I_s$ goes down monotonically. The peak brought about by the $0_{\uparrow,\downarrow}$ band become less obvious for stronger EPI (see the solid and dotted lines in Fig. 3) since the spectral weights of these bands are reduced (see Fig. 4).

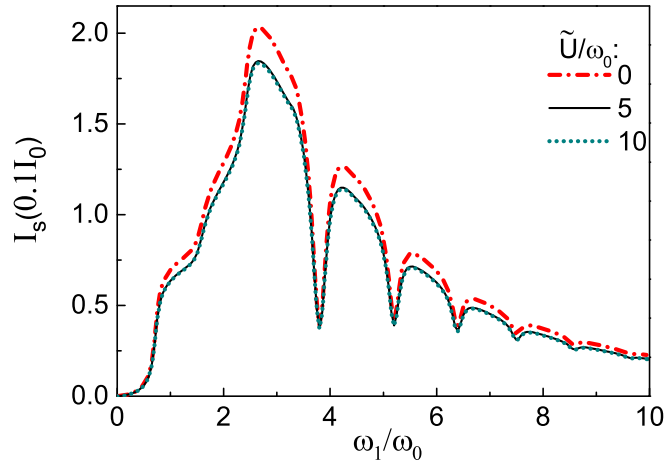


FIG. 7. Spin current dependence of Coulomb interaction $\widetilde{U}$ for $g\mu_B B_1 = 1.2\omega_0$. Other parameters are as in Fig. 1.

From the discussion above we see that the biggest spin current does not always appear at the resonant rotating frequency $\omega_1 = \omega_r$. The location is decided by several factors, such as $\lambda$ and $g\mu_B B_1$.

As plotted in Fig. 5, the effect of the electronic coupling strength $\Gamma$ on the spin current is evaluated. By improving the electronic coupling, electron tunneling into and out of the QD is facilitated. However, for enhanced coupling the spin current in the system considered may not increase as expected. With increasing $\Gamma$ the spin current of the system declines sharply at $g\mu_B B_1 = 0.2\omega_0$ [see Fig. 5(a)] but goes up greatly at $g\mu_B B_1 = 3.2\omega_0$ [see Fig. 5(b)]. The reason behind this amazing phenomenon is the destructive interference discussed above. Figures 6(a) and 6(b) show spectral functions of the QD electron at $g\mu_B B_1 = 0.2\omega_0$ and $\omega_1 = \omega_r$. Compared with Fig. 6(a), an important difference in Fig. 6(b) is that the

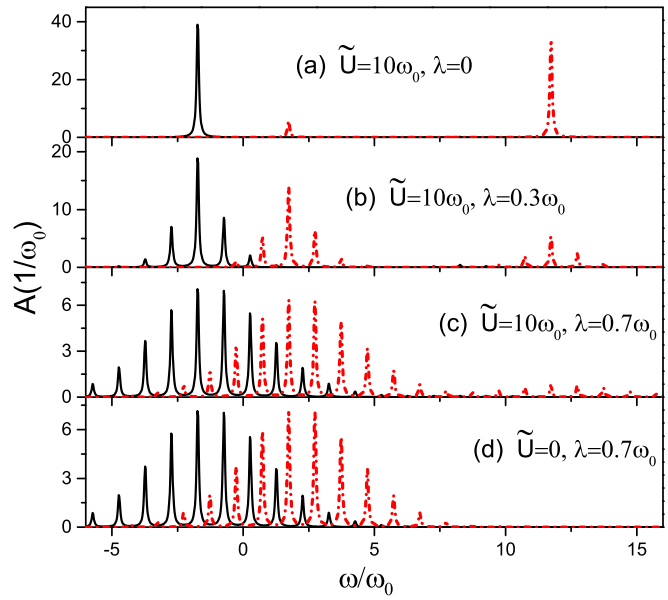


FIG. 8. The dimensionless spectral functions of the QD electron of spin up (solid line) and spin down (dash-dotted line) for, in units of $\omega_0$, $\widetilde{U} = 0, 10$, $\lambda = 0, 0.3, 0.7$ at $g\mu_B B_1 = 1.2$ and $\omega_1 = 4.5$. Other parameters are as in Fig. 7.

overlap between spectral functions of different spins expands significantly, which leads to a big increase in the intension of the destructive interference. This is why the main peak in Fig. 5(a) goes down for rising $\Gamma$. For large $g\mu_B B_1$, say, $g\mu_B B_1 = 3.2\omega_0$, the QD levels $\tilde{\varepsilon}^{rf}_{c\downarrow,\uparrow}$ are far away from each other. So with rising $\Gamma$ there is no significant increase in the spectral functions overlap, as can be seen from Figs. 6(c) and 6(d), and then $I_s$ in Fig. 5(b) goes up.

In the case of nonvanishing effective charge energy, $\widetilde{U} \neq 0$, the retarded Green's function $\mathbf{g}^r(\omega)$ for the isolated dot is, instead of Eqs. (13) and (14),

$$g^r_{\sigma\sigma'}(\omega) = \delta_{\sigma\sigma'} \sum_{n=-\infty}^{\infty} L_n \left( \frac{n_{\bar{\sigma}}}{\omega - \tilde{\varepsilon}^{rf}_{c\sigma} - n\omega_0 - \widetilde{U} + i0^+} + \frac{1 - n_{\bar{\sigma}}}{\omega - \tilde{\varepsilon}^{rf}_{c\sigma} - n\omega_0 + i0^+} \right). \quad (17)$$

In achieving Eq. (17), the difference between $N_{\rm ph}$ and $N_{\rm ph} + 1$ in the expression of $\Phi(t)$ has been ignored. Such approximation works well in our study, which does not require extremely low phonon temperatures. Following the same method as that to obtain Eq. (16), we get the spin current through the QD with finite $\widetilde{U}$.

Figure 7 shows the spin current $I_s$ as a function of rotating frequency $\omega_1$ for both vanishing and nonvanishing charge energy cases. $I_s$ exhibits the same properties for both cases, except decreasing spin current peaks for increasing $\widetilde{U}$. This is because for the same EPI strength the spectral weight distribution contributing to the spin current is the same, except descending spectral peaks for rising $\widetilde{U}$ [see Figs. 8(c) and 8(d)]. The EPI transfers spectral weight from the bands around $\tilde{\varepsilon}^{rf}_{c\sigma} + \widetilde{U}$ to bands around $\tilde{\varepsilon}^{rf}_{c\sigma}$, as shown in Fig. 8. The stronger the EPI is, the larger the weight transferred is because of the smaller occupation number at $\tilde{\varepsilon}^{rf}_{c\sigma}$.

## IV. CONCLUSIONS

In summary, we have investigated the spin current via an electron-phonon coupled quantum dot exposed to a rotating magnetic field and coupled to a normal-metal lead. Both vanishing and nonvanishing charge energy cases were discussed. When the electron phonon interaction is strong enough, antiresonances are generated in the spin current at Rabi frequencies of an integral number of the phonon frequency. This antiresonance is attributed to destructive interference between electron tunneling waves through different spin channels. Due to this destructive interference, the spin current may decline for increasing electronic coupling between the dot and the electron reservoir. The spin current in the system is decided by (1) the total spectral weight contributing to the electron tunneling process, (2) the intensity of the destructive interference, and (3) the probability amplitude for an electron to get spin flipped as it traverses the QD. Therefore, its main peak is not always at the resonant rotating frequency.

## ACKNOWLEDGMENTS

We would like to thank M. Yang for useful discussions. This work was financially supported by the National Natural Science Foundation of China (Grant No. 11764023).

[1] S. T. Weber and B. Rethfeld, Phys. Rev. B **99**, 174314 (2019).
[2] P. P. Aseev, P. Marra, P. Stano, J. Klinovaja, and D. Loss, Phys. Rev. B **99**, 205435 (2019).
[3] R. Härtle and M. Kulkarni, Phys. Rev. B **91**, 245429 (2015).
[4] P. Roura-Bas, L. Tosi, and A. A. Aligia, Phys. Rev. B **87**, 195136 (2013).
[5] S. Walter, B. Trauzettel, and T. L. Schmidt, Phys. Rev. B **88**, 195425 (2013).
[6] S. Hughes, P. Yao, F. Milde, A. Knorr, D. Dalacu, K. Mnaymneh, V. Sazonova, P. J. Poole, G. C. Aers, J. Lapointe, R. Cheriton, and R. L. Williams, Phys. Rev. B **83**, 165313 (2011).
[7] T. Koch, J. Loos, A. Alvermann, and H. Fehske, Phys. Rev. B **84**, 125131 (2011).
[8] T. Koch, J. Loos, A. Alvermann, A. R. Bishop, and H. Fehske, J. Phys.: Conf. Ser. **220**, 012014 (2010).
[9] R. C. Monreal and A. Martin-Rodero, Phys. Rev. B **79**, 115140 (2009).
[10] M. Galperin, M. A. Ratner, and A. Nitzan, J. Phys.: Condens. Matter **19**, 103201 (2007).
[11] D. M.-T. Kuo and Y. C. Chang, Phys. Rev. B **66**, 085311 (2002).
[12] N. S. Wingreen, K. W. Jacobsen, and J. W. Wilkins, Phys. Rev. Lett. **61**, 1396 (1988); **61**, 2633 (1988).
[13] V. J. Goldman, D. C. Tsui, and J. E. Cunningham, Phys. Rev. B **36**, 7635 (1987).
[14] Z. Z. Chen, R. Lü, and B. F. Zhu, Phys. Rev. B **71**, 165324 (2005).
[15] J. Fransson and J. X. Zhu, Phys. Rev. B **78**, 113307 (2008).
[16] S. Ballmann, W. Hieringer, R. Härtle, P. Coto, M. Bryce, A. Görling, M. Thoss, and H. B. Weber, Phys. Status Solidi B **250**, 2452 (2013).
[17] D. Secker, S. Wagner, S. Ballmann, R. Härtle, M. Thoss, and H. B. Weber, Phys. Rev. Lett. **106**, 136807 (2011).
[18] S. Ballmann, W. Hieringer, D. Secker, Q. Zheng, J. A. Gladysz, A. Görling, and H. B. Weber, Chem. Phys. Chem. **11**, 2256 (2010).
[19] X. H. Qiu, G. V. Nazin, and W. Ho, Phys. Rev. Lett. **92**, 206102 (2004).
[20] N. P. de Leon, W. Liang, Q. Gu, and H. Park, Nano Lett. **8**, 2963 (2008).
[21] A. N. Pasupathy, J. Park, C. Chang, A. V. Soldatov, S. Lebedkin, R. C. Bialczak, J. E. Grose, L. A. K. Donev, J. P. Sethna, D. C. Ralph, and P. L. McEuen, Nano Lett. **5**, 203 (2005).
[22] J. Repp, P. Liljeroth, and G. Meyer, Nat. Phys. **6**, 975 (2010).
[23] A. K. Hüttel, B. Witkamp, M. Leijnse, M. R. Wegewijs, and H. S. J. van der Zant, Phys. Rev. Lett. **102**, 225501 (2009).
[24] J. Hihath, C. Bruot, and N. Tao, ACS Nano **4**, 3823 (2010).
[25] H. Haug and A. P. Jauho, *Quantum Kinetics in Transport and Optics of Semiconductor* (Springer, Berlin, 1998), pp. 162–166.
[26] G. D. Mahan, *Many-Particle Physics*, 3rd ed. (Plenum, New York, 2000), pp. 218–228.